Field-induced spin reorientation in the Néel-type antiferromagnet $MnPS_3$

Hui Han,[1,*] Hong Lin,[1,*] Wei Gan,[1] Ruichun Xiao,[1] Yucheng Liu,[1] Jiefeng Ye,[1] Limin Chen,[2] Weiwei Wang,[1] Lei Zhang,[3] Changjin Zhang,[1,3,†] and Hui Li[1,†]

[1]*Information Materials and Intelligent Sensing Laboratory of Anhui Province, Institutes of Physical Science and Information Technology, Anhui University, Hefei 230601, China*

[2]*Advanced Electromagnetic Information Materials and Devices Research Center, Nanjing University of Posts and Telecommunications, Nanjing 210023, China*

[3]*Anhui Key Laboratory of Condensed Matter Physics at Extreme Conditions, High Magnetic Field Laboratory of Anhui Province, Hefei Institutes of Physical Science, Chinese Academy of Sciences, Hefei 230031, China*

(Received 19 October 2022; revised 16 January 2023; accepted 30 January 2023; published 17 February 2023)

Manipulation of spin orientation in magnetic material has been the focus of increasing research interest, as it brings fascinating perspectives with regard to the exploration of underlying magnetic interactions and the design of electronic devices. Here we report on the field-induced spin reorientation below Néel temperature in antiferromagnet $MnPS_3$. The ferromagnetic ordering emerges in the antiferromagnetic phase in $MnPS_3$ at temperatures below ∼34 K with external magnetic fields up to ∼2 kOe. Such a coexistence of the ferromagnetic and antiferromagnetic phases is obtained in both perpendicular ($H \perp ab$) and parallel ($H // ab$) configurations, even with strong anisotropy. The H-T phase diagram for $MnPS_3$ single crystal is further established with multiple magnetic phases being demonstrated. A phenomenological picture of the evolution of spin reorientation under external magnetic fields is proposed as physical insight into the rich magnetic properties of $MnPS_3$. Our findings examine an exciting frontier in fundamental investigations of low-dimensional antiferromagnets and open a path towards the realization of conceptual electronic devices.

DOI: 10.1103/PhysRevB.107.075423

I. INTRODUCTION

Spin orientation plays a foundational role in determining the ground states of magnetic systems. Layered transition-metal phosphorous trichalcogenides MPX_3 (where M = Mn, Fe, etc., X = S, Se) with exceptional physical properties have provided a promising playground for physical insight into the relationship between spin orientation and magnetic ground states under various stimulations [1–6]. The spin orientation in MPX_3 is conspired by subtle competition between multiple magnetic interactions, for example, the direct M-M exchange interaction and indirect superexchange interaction between chalcogenide atoms within the intralayer and interlayer [7–13]. Mapping and engineering the spin orientation in MPX_3 may open unforeseen opportunities for the exploration of underlying physics and the two-dimensional magnetic devices application [14–17].

As a representative two-dimensional antiferromagnet, the magnetic properties of $MnPS_3$ have been widely studied recently [18–21]. $MnPS_3$ possesses a layered structure with lattice constants $a = 6.076$ Å, $b = 10.524$ Å, $c = 6.796$ Å, $\alpha = \gamma = 90°$, $\beta = 107.35°$ [19,22], forming a monoclinic crystal structure of $C2/m$ space group, as shown in Figs. 1(a) and 1(b). The intralayer is covalent bonded, while the interlayer is bonded by van der Waals force. Theoretical and experimental explorations have proved that the $MnPS_3$ features an antiferromagnetic property below Néel temperature of ∼78 K [20,21]. The nearest-neighbor interactions in each layer are antiferromagnetic, while the spin orientations are pointed towards the out-of-ab plane, deviating from the normal direction of the ab plane by ∼8° [20], as shown in Fig. 1(c). Such small deviation of ∼8° in $MnPS_3$ offers new possibilities to engineer the spin orientations under multiple controls, such as intercalation [23,24], heterostructure [25,26], magnetic field [20,27], strain [28,29], and thickness [21,30,31], which could result in fascinating physical properties with implications in fundamental research and device design.

Here we report the manipulation of spin orientation in $MnPS_3$ single crystals below Néel temperature by external magnetic fields. The nonsynchronous evolution of the spin-up and spin-down components in $MnPS_3$ single crystals has led to the emergency of ferromagnetic (FM) ordering in the antiferromagnetic (AFM) phase below ∼34 K. A phenomenological view has been further proposed to physical insight into the spin orientation and rich magnetic properties under magnetic fields in antiferromagnet $MnPS_3$.

II. EXPERIMENT

$MnPS_3$ single crystal was synthesized by the chemical vapor transport (CVT) method. Manganese powder (Aladdin, ⩾ 99.9%), phosphorus powder (Aladdin, ⩾ 98.5%), and

*These authors contributed equally to this work.
†Authors to whom correspondence should be addressed: zhangcj@hmfl.ac.cn; huili@ahu.edu.cn

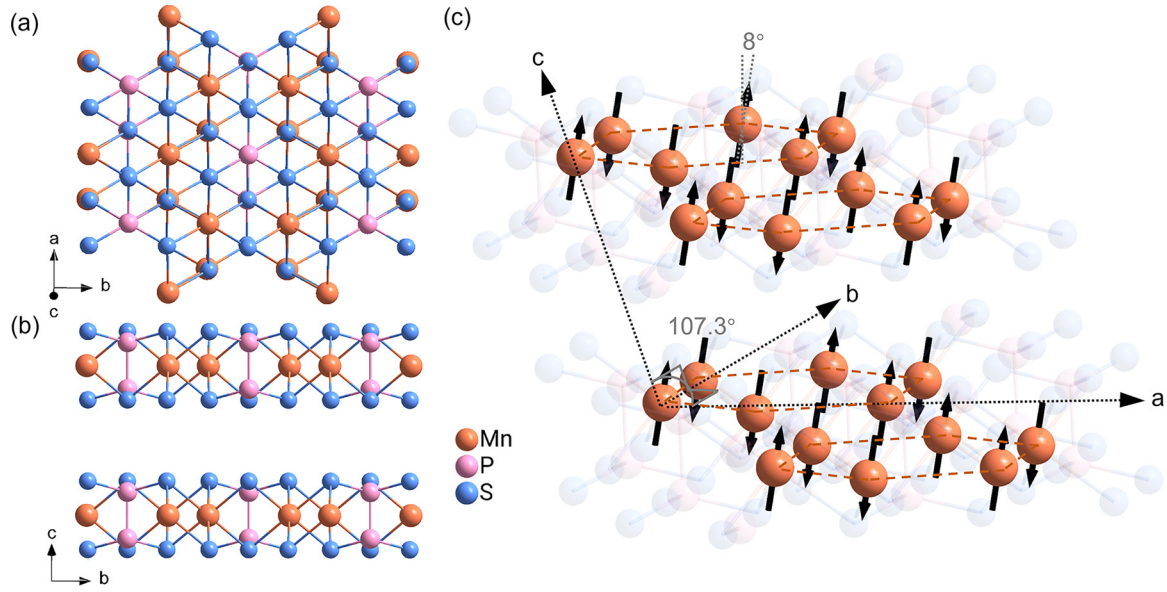

FIG. 1. Crystal and magnetic structure of $MnPS_3$: (a) top view and (b) side view of the $MnPS_3$; (c) magnetic structure of $MnPS_3$.

sulfur powder (SCR, $\geqslant$ 99.9%) were mixed in a stoichiometric ratio of 1:1:3 in the glovebox and sealed in a vacuum quartz tube. The tube was placed in a dual-temperature zone tubular furnace with the hot end at 700 K and cold end at 650 K for 3 days, and then slowly cooled to 650 K and 600 K for the hot and cold end, respectively, and kept for another 4 days. Finally, yellow transparent $MnPS_3$ crystals were obtained.

X-ray diffraction (XRD) patterns were collected by a Rigaku D Max/Ultima IV diffractometer with monochromatized Cu $K\alpha$ radiation ($\lambda = 0.154$ nm) to identify the crystal structure. The crystal morphology and elemental composition of $MnPS_3$ were characterized by scanning electron microscopy (SEM) and energy-dispersive x-ray (EDX) spectroscopy. Magnetization measurements were carried out using a Quantum Design superconducting quantum interference device-vibrating sample magnetometer (SQUID-VSM). The no-overshoot mode was adopted to ensure a precise magnetic field. Temperature dependence of magnetic susceptibilities were measured in zero-field-cooling or field-cooling modes at selected magnetic fields. All isothermal magnetization curves were measured by cooling to the target temperature under zero magnetic field after the sample was warmed to 350 K and kept for several minutes.

III. RESULTS AND DISCUSSION

Figure 2(a) shows the XRD pattern of the $MnPS_3$.The diffraction peaks are determined as $(00l)$ of single-crystal $MnPS_3$ with $C2/m$ space group (standard PDF No. 00-33-0903). The layer spacing d is calculated to be 6.535 Å from the (001) diffraction peak using Bragg's law, which is close to previous reports of 6.5 Å [32]. No other diffraction peaks are observed, which validates the high-quality nature of single-crystal $MnPS_3$. The measured EDX spectroscopy of $MnPS_3$ crystal [Fig. 2(b)] shows the calculated atomic ratio of grown $MnPS_3$ crystal is Mn : P : S = 0.939: 1.067 : 2.993, which is close to the stoichiometry of $MnPS_3$. In addition, the Mn, P, and S elements are uniformly distributed, as demonstrated by the EDX mapping result in the inset of Fig. 2(b).

The temperature dependence of magnetic susceptibility (χ-T) for single-crystal $MnPS_3$ was investigated with a magnetic field of 200 Oe being applied perpendicular and parallel to the ab plane, respectively, as shown in Fig. 3. The $MnPS_3$ exhibits multiple magnetic phase transitions as the temperature decreases from 300 to 10 K in the perpendicular configuration, *i.e.*, $H \perp ab$ plane [Fig. 3(a)]. With temperature decreasing from 300 K, the magnetic susceptibility of $MnPS_3$

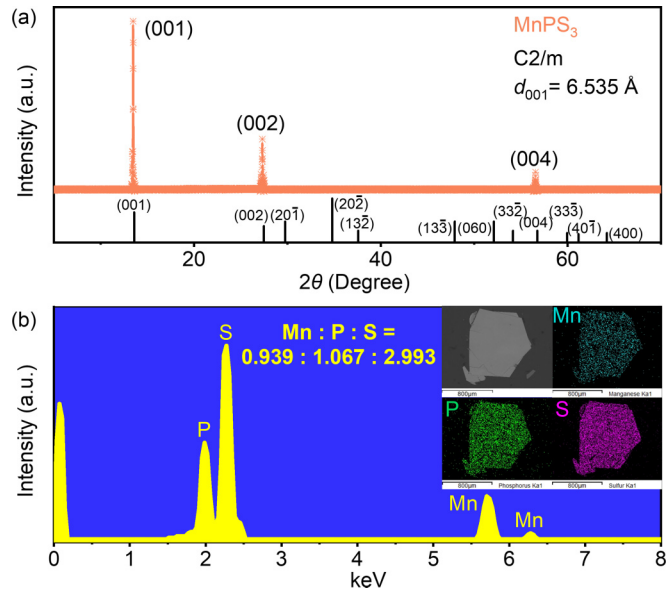

FIG. 2. (a) XRD pattern of $MnPS_3$ with $(00l)$ diffraction peaks indicated (orange curve). The bottom black lines are the diffraction peaks for $MnPS_3$ with standard PDF No. 00-33-0903. (b) EDX spectroscopy of as-grown $MnPS_3$. Inset shows the morphology image and elements mapping of $MnPS_3$ single crystal collected by SEM.

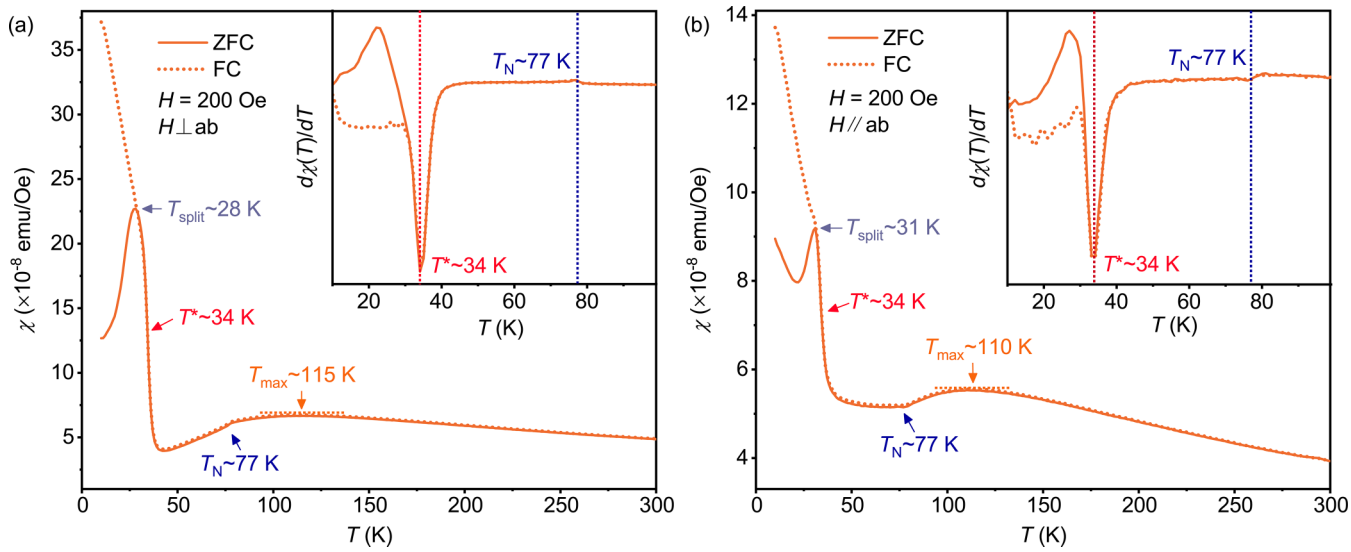

FIG. 3. Temperature dependence of magnetic susceptibility of $MnPS_3$ single crystal under ZFC (solid curve) and FC (dashed curve) with the $H \perp ab$ plane (a) and $H//ab$ plane (b), respectively. Insets show the differential curves $[d\chi(T)/dT–T]$ with the characteristic temperatures T^* and T_N indicated.

gradually increases to its extremum value at $T_{max}\sim115$ K [30] and then declines as the temperature further decreases, with a kink occurring at ∼77 K. The occurrence of a broad peak at $T_{max}\sim115$ K suggests the emergency of AFM ordering in $MnPS_3$, while the temperature for the kink at ∼77 K corresponds to the extremum value in the differential curve $[d\chi(T)/dT–T]$ in the inset of Fig. 3(a) and is defined as Néel temperature, T_N. As temperature further decreases below ∼40 K, the magnetic susceptibility of $MnPS_3$ starts to increase rapidly, which is a signature of the emergency of FM ordering [20]. The FM transition temperature is determined to be $T^*\sim34$ K, corresponding to the extremum value of curve $[d\chi(T)/dT–T]$ in the inset of Fig. 3(a). The splitting between the zero-field-cooling (ZFC, solid curve) and field-cooling (FC, dashed curve) curves occurs at $T_{split}\sim28$ K. Below the temperature, the magnetic susceptibility of $MnPS_3$ starts to decrease under ZFC and increases under FC measurements. This splitting between the ZFC and FC curves is probably related to the coexistence and competition between FM ordering and AFM ordering.

Similar multiple magnetic phase transitions are also observed in $MnPS_3$ in the parallel configuration, *i.e.*, $H//ab$ plane, except that a very weak magnetic susceptibility upturn occurs below ∼20 K in the ZFC curve. This weak upturn may arise from various magnetic scatterings from defects, grain boundaries, etc. [5,33,34]. In addition, the magnetic susceptibility of $MnPS_3$ in the $H//ab$ plane is smaller than that in the $H \perp ab$ plane, indicating that $MnPS_3$ features strong magnetic anisotropy.

To gain physical insight into the phase transition at $T^*\sim34$ K, we further measured the temperature dependence of magnetic susceptibility of $MnPS_3$ at different magnetic fields for the $H \perp ab$ plane and $H//ab$ plane, respectively, as shown in Fig. 4. Under the $H \perp ab$ plane, the magnetic susceptibility of $MnPS_3$ features a rapid increase at temperature below ∼40 K and a remarkable splitting between ZFC and FC curves at magnetic fields lower than 1 kOe [Fig. 4(a)]. The rapid increase of magnetic susceptibility is indicative of the emergency of FM ordering, as discussed above. The FM transition temperature T^* is almost unchanged with increasing external magnetic fields, as indicated by the orange spheres in the inset of Fig. 4(a). It implies that FM ordering in $MnPS_3$ is robust at low magnetic fields. In contrast, the splitting between ZFC and FC curves is significantly suppressed. The characteristic temperature T_{split} gradually decreases with increasing magnetic fields and is invisible as the magnetic field increases to 1 kOe (light green curve), as indicated by the wine spheres in the inset of Fig. 4(a), suggesting that the coexistence of the FM phase and AFM phase in $MnPS_3$ is metastable.

However, as the magnetic field further increases above 2 kOe, the emerging FM ordering at ∼34 K disappears and the AFM ordering mainly dominates. Only a sharp decrease of magnetic susceptibility is observed at temperature below T_{max} at 10 kOe (green curves) and 30 kOe (purple curves), as shown in Fig. 4(c). However, an upturn of magnetic susceptibility reoccurs at even higher magnetic field, for example, 50 kOe (light blue curves) and 70 kOe (dark blue curves) in Fig. 4(c). This upturn is related to the magnetic transition from AFM phase to forced ferromagnetic (FFM) phase under relatively high magnetic fields [29,32,35]. In addition, the magnitude of magnetic susceptibility of $MnPS_3$ experiences a nonmonotonous evolution with increasing magnetic fields. It first decreases as the magnetic field increases below 30 kOe, for example, the magnetic susceptibility is calculated to be $\sim9.7\times10^{-7}$ emu/Oe at 50 Oe and decreases by one order of magnitude to $\sim3\times10^{-8}$ emu/Oe at 30 kOe at 10 K in FC curves. Such suppression indicates that the FM ordering in $MnPS_3$ is getting weaker with increasing magnetic field. As the magnetic field further increases, the magnitude of magnetic susceptibility slightly increases to $\sim6.8\times10^{-8}$ emu/Oe at 70 kOe and 10 K, which corresponds to the formation of the FFM state. The evolution of magnetic susceptibility along with the increasing magnetic field of $MnPS_3$ in the

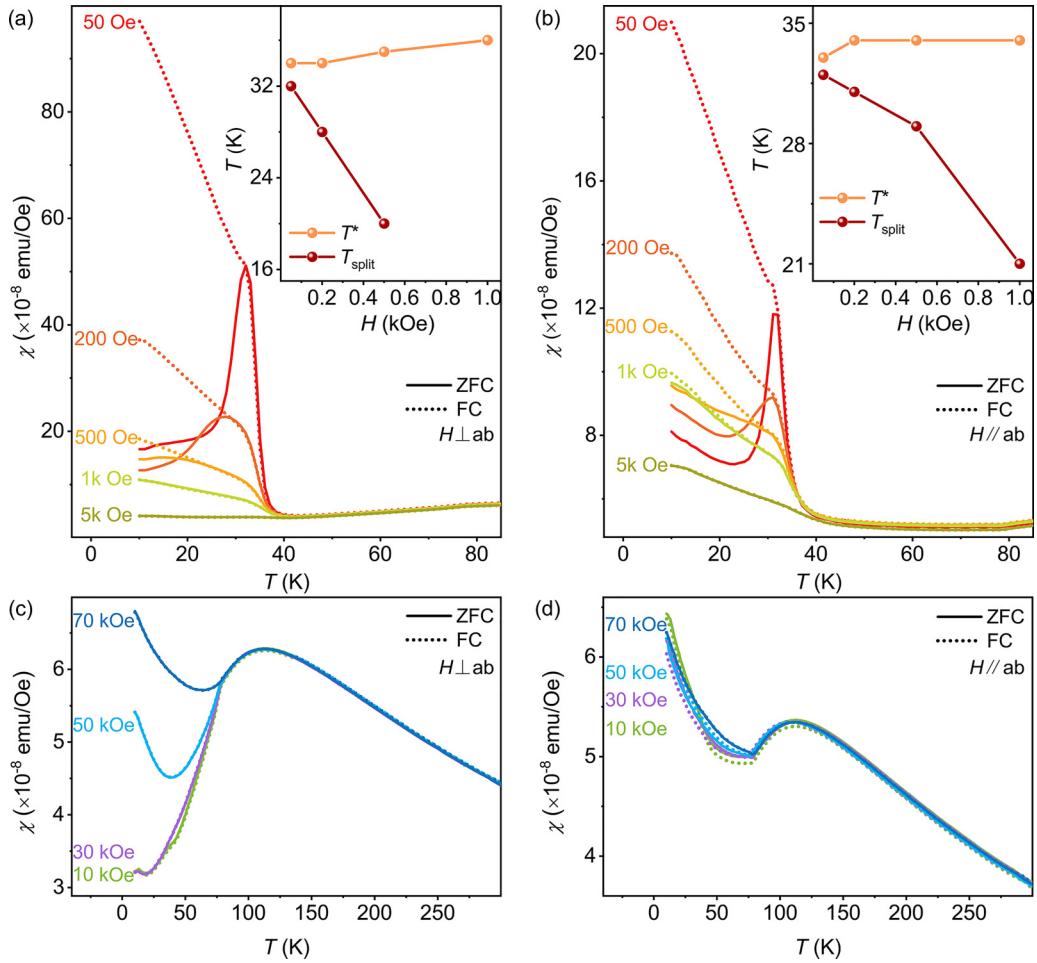

FIG. 4. Temperature dependence of magnetic susceptibility of $MnPS_3$ under different magnetic fields indicated for the $H \perp ab$ plane (a), (c) and $H//ab$ plane (b), (d), respectively. The solid and dashed curves represent the ZFC and FC measurements, respectively. The upper-right insets in (a) and (b) show the characteristic temperatures, T^* (orange spheres) and T_{split} (wine spheres), as a function of applied magnetic field.

$H//ab$ plane shares similar behaviors, as shown in Fig. 4(b) for the low magnetic field and Fig. 4(d) for the high magnetic field. The critical magnetic field for formation of the FFM state in the $H//ab$ plane is estimated to be ~10 kOe [Fig. 4(d)], in which an evident magnetic susceptibility upturn occurs below T_N. This critical magnetic field in the $H//ab$ plane is smaller than that in the $H \perp ab$ plane of ~50 kOe, which may relate to the magnetic structure of $MnPS_3$, with an easy axis being aligned roughly along the out-of-ab plane [Fig. 1(c)].

Isothermal magnetization (M-H) curves for $MnPS_3$ at selected temperatures of 10 K, 35 K, and 100 K for the $H \perp ab$ plane and $H//ab$ plane are shown in Fig. 5. The $MnPS_3$ features a distinctive anisotropic property. For the $H \perp ab$ plane in Fig. 5(a), a linear dependence of M versus H is observed at 100 K (blue curve), suggesting the formation of a paramagnetic (PM) state in $MnPS_3$. However, an evident upturn occurs at a magnetic field of ~45 kOe and ~35 kOe as the temperature further cools to 35 K (red curve) and 10 K (black curve), respectively. The upturn in isothermal magnetization above a critical magnetic field is most likely due to the spin-flop transition in $MnPS_3$, which indicates the easy axis of $MnPS_3$ is roughly normal to the ab plane and is consistent with previous studies [32,36,37]. No magnetization saturation is observed for $MnPS_3$ with the $H \perp ab$ plane, even with magnetic fields increasing to 70 kOe. In addition, an evident hysteresis loop with coercive field of ~115 Oe is observed in $MnPS_3$ at 10 K with the $H \perp ab$ plane, as indicated by the black curve in the zoom-in view in Fig. 5(b), and smears out as temperature increases above 35 K [red curve for 35 K and blue curve for 100 K in Fig. 5(b)]. The occurrence of a hysteresis loop in the M-H curves is indicative of the formation of FM ordering, which coincides with the observed magnetic phase transition at T^*~34 K in the χ-T curves in Figs. 3(a) and 4(a). Moreover, the hysteresis loop exhibits a slight shrink in the vicinity of zero magnetic moment with a very small coercive field of ~115 Oe, which suggests the FM ordering is weak and probably coexisted with AFM ordering. This also coincides with the splitting of the ZFC and FC curves at low temperatures, while for the $H//ab$ plane the M-H curves show linear behaviors at all temperatures of 10, 35, and 100 K, as shown in Fig. 5(c). The zoom-in view of Fig. 5(d) shows an unremarkable hysteresis loop at 10 K (black curve). Such hysteresis loops may arise from instrumental error or the relatively weaker FM ordering existing along the ab plane than that normal to the ab plane.

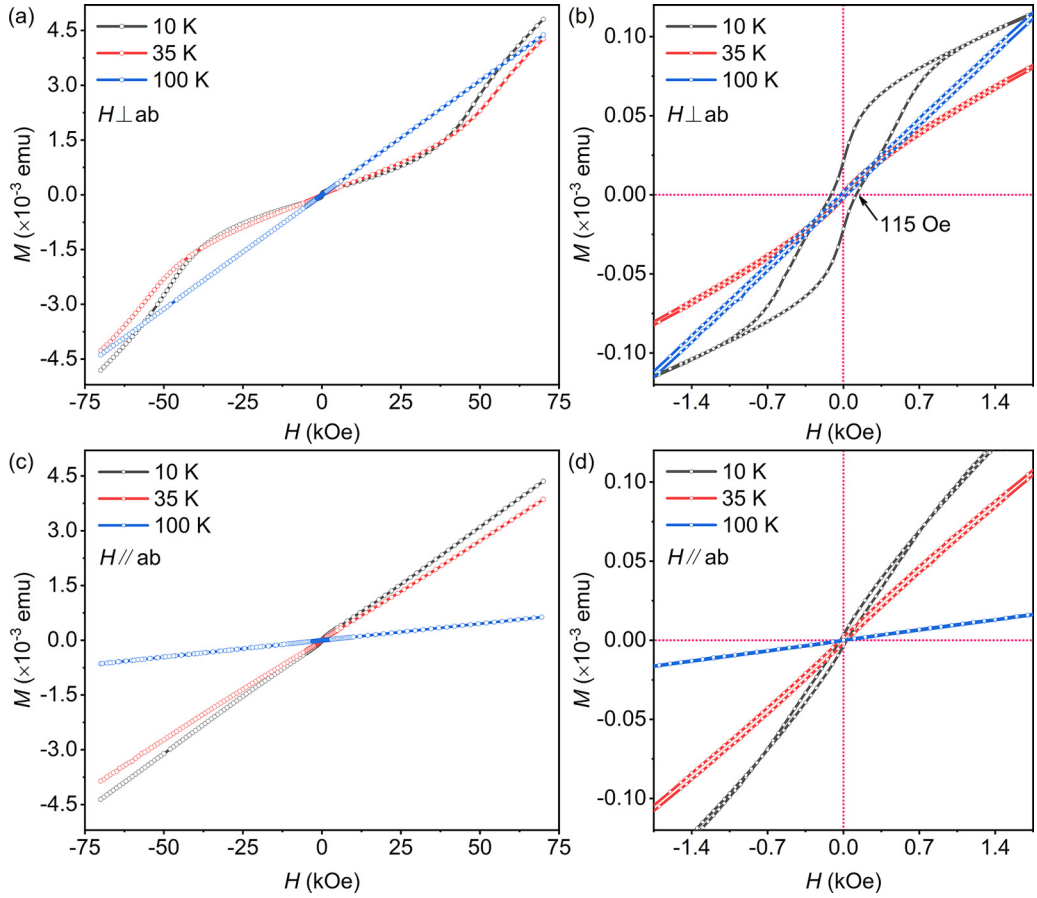

FIG. 5. M-H curves for $MnPS_3$ at different temperatures indicated (10 K, 35 K, 100 K) for the $H \perp ab$ plane (a) and $H//ab$ plane (c). Zoom-in view of M-H curves at low magnetic fields for $H \perp ab$ plane (b) and $H//ab$ plane (d), respectively.

Further increasing temperature above 35 K (red curve for 35 K and blue curve for 100 K) causes the hysteresis loop to be invisible.

Figure 6 shows the established magnetic phase diagram (H-T) of $MnPS_3$ based on the measured χ-T and M-H curves at low magnetic fields ($H < 5$ kOe) for $H \perp ab$ plane and $H//ab$ plane, respectively. At magnetic fields lower than 2 kOe, the magnetic phase diagram is divided into four different regions, which sequentially transition from the PM phase, the coexisting AFM phase and PM phase (AFM & PM), the

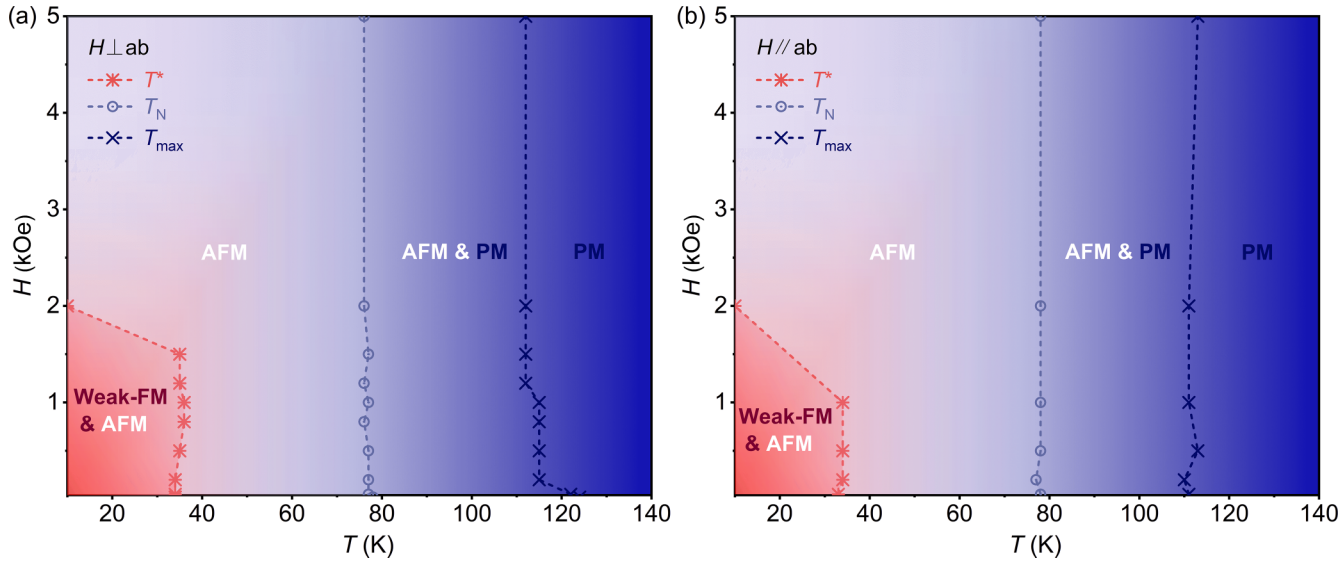

FIG. 6. H-T phase diagram of $MnPS_3$ for the $H \perp ab$ plane (a) and $H//ab$ plane (b), respectively.

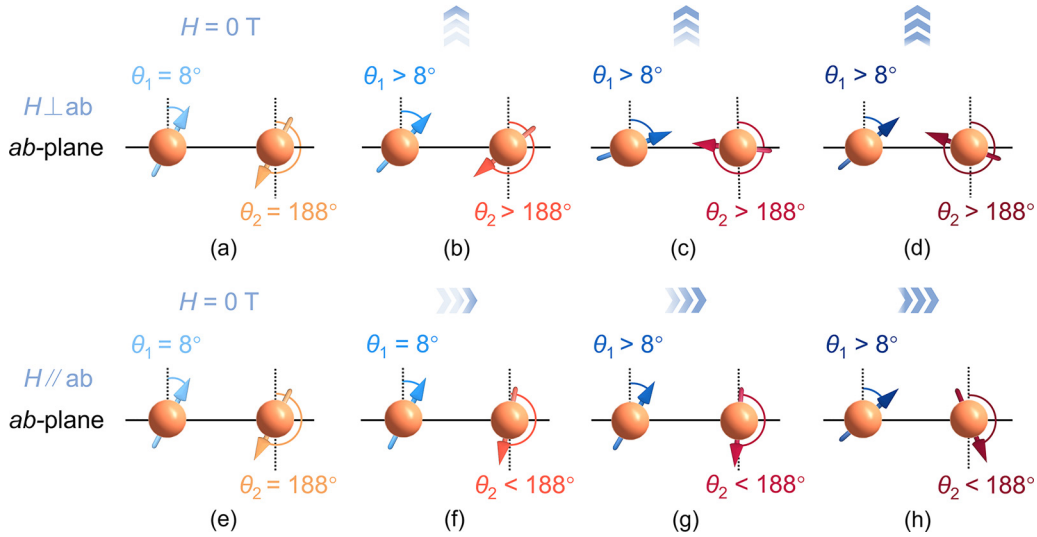

FIG. 7. Schematic diagram of evolution of spin orientation along external magnetic field for the $H \perp ab$ plane (a)–(d) and $H//ab$ plane (e)–(h), respectively. The direction and filling gradient of the top blue arrows indicate the magnetic field orientation and strength, respectively.

AFM phase, and the coexisting weak-FM phase and AFM phase (weak-FM & AFM) along with decreasing temperature from 140 to 10 K, while at the intermediate magnetic fields region, *i.e.,* 2 kOe $< H <$ 5 kOe, the coexisting weak-FM & AFM phases disappear with only three magnetic phases being left, as discussed qualitatively below. A similar magnetic phase diagram is also established for $H//ab$ plane, as shown in Fig. 6(b).

Figure 7 depicts a simplified schematic diagram of the evolution of spin orientations under the $H \perp ab$ plane [Figs. 7(a)–7(d)] and $H//ab$ plane [Figs. 7(e)–7(h)] configurations below T^*. At the initial stage with $H = 0$ Oe, the spins of neighboring Mn atoms are antiparallel aligned with spin-up (or spin-down) orientation of $\theta_1 \sim 8^\circ$ (or $\theta_2 \sim 188^\circ$) from the normal direction of the *ab* plane [Fig. 7(a)], which is the magnetic ground state proved by neutron diffraction measurements [20]. When applying a weak perpendicular magnetic field, the spin-up and spin-down components tend to rotate towards the *ab* plane with $\theta_1 > 8^\circ$ and $\theta_2 > 188^\circ$, as indicated by Fig. 7(b). Such rotation behavior is believed to be a consequence of the competition between the external magnetic field and magnetic anisotropy of $MnPS_3$. The antiparallel alignment between the spin-up and spin-down components is roughly maintained at small external magnetic field due to the magnetic anisotropy field and strong AFM interaction between the nearest Mn ions in $MnPS_3$ [10,36,38–40]. However, the rotation of the spin-up and spin-down components is nonsynchronized, which results in the existence of net magnetization, as evidenced from the occurrence of FM ordering from the χ-T curves in Figs. 3(a) and 4(a) at temperatures below $T^* \sim 34$ K and the emergency of the narrow hysteresis loop in the M-H curve at 10 K in Fig. 5(b). As the strength of the perpendicular magnetic field increases, the spin-up and spin-down components are gradually aligned parallel to the *ab* plane, as shown in Fig. 7(c). This corresponds to the spin-flop process occurring at critical magnetic field, as demonstrated from the M-H curves in Fig. 5(a). In addition, the AFM ordering dominates under this situation, which coincides with the experimental measured χ-T curves collected at $H = 10$ kOe and 30 kOe in Fig. 4(c). Further increasing perpendicular magnetic fields, both the spin-up and spin-down components are rotated towards the direction of the external magnetic fields with opposite rotation direction, *i.e.*, counterclockwise for the spin-up component and clockwise for the spin-down component, as demonstrated in Fig. 7(d). This relates to the emergency of the FFM state, which is consistent with experimental measurements of the χ-T curves in Fig. 4(c) with magnetic field above 50 kOe. It is noted that reversal of spin direction for the spin-down component occurs with increasing perpendicular magnetic field, as illustrated in Figs. 7(c) and 7(d). Moreover, the nonsaturation behavior in the M-H curves of $MnPS_3$ [Fig. 5(a)] suggests that the spins are not well aligned parallel to the external field, even at high magnetic fields of 70 kOe [Fig. 7(d)].

The evolution of spin orientation along with parallel magnetic field is depicted in Figs. 7(e)–7(h). Figure 7(e) is the magnetic ground state with the same configuration in Fig. 7(a). With increasing parallel magnetic field, the spin-up component and spin-down component are both rotated in the direction of the external magnetic fields [Figs. 7(f)–7(h)]. The rotation direction of the spin-up and spin-down components is opposite one another, *i.e.*, clockwise for the spin-up component and counterclockwise for the spin-down component. The nonsynchronized rotation between the spin-up and spin-down components at small parallel magnetic field may give rise to the occurrence of weak FM ordering [Figs. 7(f) and 7(g)], as evidenced from the χ-T curves in Figs. 3(b) and 4(b). With further increasing strength of parallel magnetic fields, the spin-down component gradually crosses the normal line of the *ab* plane [Fig. 7(h)], which may result in the emergency of an FFM state in $MnPS_3$, as evidenced from the measured χ-T curves in Fig. 4(d). It should be noted that although the suspected phenomenological picture of the evolution of spin rotation may account for most of the intriguing observations in our $MnPS_3$ system, the quest for further

theoretical and experimental investigations have remained a demanding challenge.

IV. CONCLUSION

We have systematically studied the magnetic properties of antiferromagnet $MnPS_3$. A weak FM ordering is observed at temperatures below $T^*\sim34$ K at magnetic fields lower than 2 kOe in both the $H\perp ab$ plane and $H//ab$ plane configurations. The splitting between the ZFC and FC curves further suggests the weak short-range FM ordering is metastable and coexists with AFM ordering. In addition, the weak FM ordering is suppressed with increasing external magnetic fields. The H-T phase diagram for $MnPS_3$ is further established with various magnetic phases being obtained, including the coexisting weak-FM phase and AFM phase, the AFM phase, the coexisting AFM phase and PM phase, and the PM phase. A phenomenological picture of the evolution of spin reorientation under external magnetic fields has been further proposed as physical insight into the rich magnetic properties of antiferromagnet $MnPS_3$ qualitatively. Our findings may stimulate new perspectives for fundamental investigations of low-dimensional antiferromagnets and afford the realization of proof-of-concept devices with potential practical applications in advanced integrated circuits.

ACKNOWLEDGMENTS

This work was supported in part by the National Natural Science Foundation of China under Grants No. 11904001, No. 11904004, and No. 12074386, in part by the Joint Funds of the National Natural Science Foundation of China and the Chinese Academy of Sciences Large-Scale Scientific Facility under Grant No. U1932156, in part by the Natural Science Foundation of Anhui Province under Grant No. 2008085QA29, and in part by the Anhui Innovation Project under Grant No. 2021LCX007.

[1] X. Li, X. Wu, and J. Yang, Half-metallicity in $MnPSe_3$ exfoliated nanosheet with carrier doping, J. Am. Chem. Soc. **136**, 11065 (2014).

[2] M. A. Susner, M. Chyasnavichyus, M. A. McGuire, P. Ganesh, and P. Maksymovych, Metal thio- and selenophosphates as multifunctional van Der Waals layered materials, Adv. Mater. **29**, 1602852 (2017).

[3] F. Kargar, E. A. Coleman, S. Ghosh, J. Lee, M. J. Gomez, Y. Liu, A. S. Magana, Z. Barani, A. Mohammadzadeh, B. Debnath, R. B. Wilson, R. K. Lake, and A. A. Balandin, Phonon and thermal properties of quasi-two-dimensional $FePS_3$ and $MnPS_3$ antiferromagnetic semiconductors, ACS Nano **14**, 2424 (2020).

[4] M. J. Coak, D. M. Jarvis, H. Hamidov, A. R. Wildes, J. A. M. Paddison, C. Liu, C. R. S. Haines, N. T. Dang, S. E. Kichanov, B. N. Savenko, S. Lee, M. Kratochvílová, S. Klotz, T. C. Hansen, D. P. Kozlenko, J.-G. Park, and S. S. Saxena, Emergent Magnetic Phases in Pressure-Tuned van der Waals Antiferromagnet $FePS_3$, Phys. Rev. X **11**, 011024 (2021).

[5] R. Basnet, K. M. Kotur, M. Rybak, C. Stephenson, S. Bishop, C. Autieri, M. Birowska, and J. Hu, Controlling magnetic exchange and anisotropy by nonmagnetic ligand substitution in layered MPX_3 (M = Ni, Mn; X = S, Se), Phys. Rev. Res. **4**, 023256 (2022).

[6] M. Mi, X. Zheng, S. Wang, Y. Zhou, L. Yu, H. Xiao, H. Song, B. Shen, F. Li, L. Bai, Y. Chen, S. Wang, X. Liu, and Y. Wang, Variation between antiferromagnetism and ferrimagnetism in $NiPS_3$ by electron doping, Adv. Funct. Mater. **32**, 2112750 (2022).

[7] K. A. Yagotintsev, M. A. Strzhemechny, A. I. Prokhvatilov, Yu. E. Stetsenko, and Yu. M. Vysochanskii, Interlayer Mn–Mn exchange parameter in $MnPS_3$ from x-ray diffraction data, Low Temp. Phys. **38**, 493 (2012).

[8] N. Sivadas, M. W. Daniels, R. H. Swendsen, S. Okamoto, and D. Xiao, Magnetic ground state of semiconducting transition-metal trichalcogenide monolayers, Phys. Rev. B **91**, 235425 (2015).

[9] B. L. Chittari, Y. Park, D. Lee, M. Han, A. H. MacDonald, E. Hwang, and J. Jung, Electronic and magnetic properties of single-layer MPX_3 metal phosphorous trichalcogenides, Phys. Rev. B **94**, 184428 (2016).

[10] J. Yang, Y. Zhou, Q. Guo, Y. Dedkov, and E. Voloshina, Electronic, magnetic and optical properties of $MnPX_3$ (X = S, Se) monolayers with and without chalcogen defects: A first-principles study, RSC Adv. **10**, 851 (2020).

[11] N. Bazazzadeh, M. Hamdi, S. Park, A. Khavasi, S. M. Mohseni, and A. Sadeghi, Magnetoelastic coupling enabled tunability of magnon spin current generation in 2D antiferromagnets, Phys. Rev. B **104**, L180402 (2021).

[12] H.-J. Koo, R. Kremer, and M.-H. Whangbo, Unusual spin exchanges mediated by the molecular anion $P_2S_6^{4-}$: Theoretical analyses of the magnetic ground states, magnetic anisotropy and spin exchanges of MPS_3 (M = Mn, Fe, Co, Ni), Molecules **26**, 1410 (2021).

[13] C. Autieri, G. Cuono, C. Noce, M. Rybak, K. M. Kotur, C. E. Agrapidis, K. Wohlfeld, and M. Birowska, Limited ferromagnetic interactions in monolayers of MPS_3 (M = Mn and Ni), J. Phys. Chem. C **126**, 6791 (2022).

[14] F. Wang, T. A. Shifa, P. Yu, P. He, Y. Liu, F. Wang, Z. Wang, X. Zhan, X. Lou, F. Xia, and J. He, New frontiers on van Der Waals layered metal phosphorous trichalcogenides, Adv. Funct. Mater. **28**, 1802151 (2018).

[15] R. Kumar, R. N. Jenjeti, and S. Sampath, Bulk and few-layer 2D, p-$MnPS_3$ for sensitive and selective moisture sensing, Adv. Mater. Interfaces **6**, 1900666 (2019).

[16] R.-C. Xiao, D.-F. Shao, Y.-H. Li, and H. Jiang, Spin photogalvanic effect in two-dimensional collinear antiferromagnets, npj Quantum Mater. **6**, 35 (2021).

[17] S. Yang, T. Zhang, and C. Jiang, Van der Waals magnets: Material family, detection and modulation of magnetism, and perspective in spintronics, Adv. Sci. **8**, 2002488 (2021).

[18] K. Kurosawa, S. Saito, and Y. Yamaguchi, Neutron diffraction study on $MnPS_3$ and $FePS_3$, J. Phys. Soc. Jpn. **52**, 3919 (1983).

[19] N. Ismail, Y. M. Temerk, A. A. El-Meligi, M. A. Badr, and M. Madian, Synthesis and characterization of $MnPS_3$ for hydrogen sorption, J. Solid State Chem. **183**, 984 (2010).

[20] E. Ressouche, M. Loire, V. Simonet, R. Ballou, A. Stunault, and A. Wildes, Magnetoelectric $MnPS_3$ as a candidate for ferrotoroidicity, Phys. Rev. B **82**, 100408(R) (2010).

[21] K. Kim, S. Y. Lim, J. Kim, J.-U. Lee, S. Lee, P. Kim, K. Park, S. Son, C.-H. Park, J.-G. Park, and H. Cheong, Antiferromagnetic ordering in van der Waals 2D magnetic material $MnPS_3$ probed by Raman spectroscopy, 2D Mater. **6**, 041001 (2019).

[22] Z. ur Rehman, Z. Muhammad, O. Adetunji Moses, W. Zhu, C. Wu, Q. He, M. Habib, and L. Song, Magnetic isotropy/anisotropy in layered metal phosphorous trichalcogenide MPS_3 (M = Mn, Fe) single crystals, Micromachines **9**, 292 (2018).

[23] X. Zhang, X. Su, H. Zhou, Y. Fu, X. Chen, C. Yang, J. Qin, M. Inokuchi, and M. Kinoshita, Synthesis and magnetic characterization of TTM-TTF intercalated into lamellar $MnPS_3$, Synth. Met. **152**, 485 (2005).

[24] X. Yan, X. Chen, and J. Qin, Synthesis and magnetic properties of layered $MnPS_xSe_{3-x}$ ($0 < x < 3$) and corresponding intercalation compounds of 2,2′-bipyridine, Mater. Res. Bull. **46**, 235 (2011).

[25] G. Hu, Y. Zhu, J. Xiang, T.-Y. Yang, M. Huang, Z. Wang, Z. Wang, P. Liu, Y. Zhang, C. Feng, D. Hou, W. Zhu, M. Gu, C.-H. Hsu, F.-C. Chuang, Y. Lu, B. Xiang, and Y.-L. Chueh, Antisymmetric magnetoresistance in a van der Waals antiferromagnetic/ferromagnetic layered $MnPS_3/Fe_3GeTe_2$ stacking heterostructure, ACS Nano **14**, 12037 (2020).

[26] H. Dai, H. Cheng, M. Cai, Q. Hao, Y. Xing, H. Chen, X. Chen, X. Wang, and J.-B. Han, Enhancement of the coercive field and exchange bias effect in $Fe_3GeTe_2/MnPX_3$ (X = S and Se) van der Waals heterostructures, ACS Appl. Mater. Interfaces **13**, 24314 (2021).

[27] D. J. Goossens, A. R. Wildes, C. Ritter, and T. J. Hicks, Ordering and the nature of the spin flop phase transition in $MnPS_3$, J. Phys.: Condens. Matter **12**, 1845 (2000).

[28] P. Sen and R. K. Chouhan, Electronic structure of MPX_3 trichalcogenide monolayers in density functional theory: A case study with four compounds (M = Mn, Fe; X = S, Se), Electron. Struct. **2**, 025003 (2020).

[29] H. Zhang, C. Niu, J. Zhang, L. Zou, Z. Zeng, and X. Wang, Spin-crossover induced ferromagnetism and layer stacking-order change in pressurized 2D antiferromagnet $MnPS_3$, Phys. Chem. Chem. Phys. **23**, 9679 (2021).

[30] Y.-J. Sun, Q.-H. Tan, X.-L. Liu, Y.-F. Gao, and J. Zhang, Probing the magnetic ordering of antiferromagnetic $MnPS_3$ by Raman spectroscopy, J. Phys. Chem. Lett. **10**, 3087 (2019).

[31] Z. Ni, H. Zhang, D. A. Hopper, A. V. Haglund, N. Huang, D. Jariwala, L. C. Bassett, D. G. Mandrus, E. J. Mele, C. L. Kane, and L. Wu, Direct Imaging of Antiferromagnetic Domains and Anomalous Layer-Dependent Mirror Symmetry Breaking in Atomically Thin $MnPS_3$, Phys. Rev. Lett. **127**, 187201 (2021).

[32] G. Long, H. Henck, M. Gibertini, D. Dumcenco, Z. Wang, T. Taniguchi, K. Watanabe, E. Giannini, and A. F. Morpurgo, Persistence of magnetism in atomically thin $MnPS_3$ crystals, Nano Lett. **20**, 2452 (2020).

[33] I. M. Alliati, R. F. L. Evans, K. S. Novoselov, and E. J. G. Santos, Relativistic domain-wall dynamics in van der Waals antiferromagnet $MnPS_3$, npj Comput. Mater. **8**, 1 (2022).

[34] Z. Lu, X. Yang, L. Huang, X. Chen, M. Liu, J. Peng, S. Dong, and J.-M. Liu, Evolution of magnetic phase in two-dimensional van der Waals $Mn_{1-x}Ni_xPS_3$ single crystals, J. Phys. Condens. Matter **34**, 354005 (2022).

[35] R. Basnet, A. Wegner, K. Pandey, S. Storment, and J. Hu, Highly sensitive spin-flop transition in antiferromagnetic van der Waals material MPS_3 (M = Ni and Mn), Phys. Rev. Mater. **5**, 064413 (2021).

[36] D. J. Goossens, Dipolar anisotropy in quasi-2D honeycomb antiferromagnet $MnPS_3$, Eur. Phys. J. B **78**, 305 (2010).

[37] Y. Zhang, W. Wang, M. Huang, P. Liu, G. Hu, C. Feng, X. Lei, M. Gu, H. Yang, K. Liu, B. Xiang, and Y. Lu, $MnPS_3$ spin-flop transition-induced anomalous Hall effect in graphite flake via van der Waals proximity coupling, Nanoscale **12**, 23266 (2020).

[38] A. R. Wildes, B. Roessli, B. Lebech, and K. W. Godfrey, Spin waves and the critical behaviour of the magnetization in $MnPS_3$, J. Phys.: Condens. Matter **10**, 6417 (1998).

[39] T. Babuka, M. Makowska-Janusik, A. V. Peschanskii, K. E. Glukhov, S. L. Gnatchenko, and Yu. M. Vysochanskii, Electronic and vibrational properties of pure $MnPS_3$ crystal: Theoretical and experimental investigation, Comput. Mater. Sci. **177**, 109592 (2020).

[40] T. Olsen, Magnetic anisotropy and exchange interactions of two-dimensional $FePS_3$, $NiPS_3$ and $MnPS_3$ from first principles calculations, J. Phys. D: Appl. Phys. **54**, 314001 (2021).